Biointerface Research in Applied Chemistry
Open-Access Journal (ISSN: 2069-5837)

Article
Volume 13, Issue 2, 2023, 162
https://doi.org/10.33263/BRIAC132.162

Phenolic Compounds in Black Grape by the Electronic and Thermochemical Studies

Fatemeh Mollaamin [1,*]

[1] Department of Biomedical Engineering, Faculty of Engineering and Architecture, Kastamonu University, Kastamonu, Turkey
* Correspondence: smollaamin@gmail.com (F.M.);

Scopus Author ID 35848813100
Received: 26.01.2022; Accepted: 4.03.2022; Published: 29.03.2022

Abstract: This investigation analyzes the effects of light and genotype on the biosynthesis of anthocyanins. The applied plant material, including dye grape varieties, accumulates anthocyanins in the skin and the pulp and hybrid populations. Anthocyanins are secondary plant metabolites with the response of most of the red to purple pigmentation existing in fruits, vegetables, and flowers. During grape berry development, these compounds are accumulated from maturation until ripening and are responsible for pigmentation found in red skin berries. Several cations linked to anthocyanins in H_2O molecules have been investigated for studying the color difference of various compounds in the low limitations of pH value. In this accomplishment, cations attached to Mal, Peo, Del, Pet, and Cya in water has been simulated, converting flavylium cations to the blue quinonoidal bases at a lower amount of pH using the IR approach by installing the beer-lambert law for getting the physicochemical properties of absorbance, intensity and of the structures. The changes of enthalpy between complexes of anthocyanins-cations have been discussed due to carbonyl groups and double bonds by the (B)-ring chelated of cyanidin, delphinidin, and petunidin anthocyanins in different media of gas and water which illustrates the stability and color of anthocyanin-cations chelated to Mal, Peo, Del, Pet, and Cya colorful pigments in a weakly acidic medium.

Keywords: black grape; anthocyanins; cation metal chelation; water.

1. Introduction

Numerous studies [1,2] have shown positive effects linked to human health of phenolic compounds extracted from the skins and seeds of grapes and winemaking by-products such as pomace. In addition to their antioxidant properties, phenolic compounds also exhibit anti-inflammatory, anticarcinogenic and neuroprotective activities [3-10]. In addition, effects on improving the cardiovascular system and decreased hypertension, a positive effect on oral health, and decreased wound healing time have been shown. These beneficial effects on human health are generally associated with condensed tannins, anthocyanins, and stilbenes [11-17].

The term anthocyanin, derived from the Greek words: flower and blue (anthos = flower, kianos = blue), was coined by Marquart in 1835 to refer to the blue pigments of flowers. It was noted later that in addition to the color blue, anthocyanins are also responsible for the colors purple, violet, magenta, and almost all shades of red that appear on flowers, fruits, leaves, stems, and roots. Anthocyanins are part of the flavonoid family and absorb visible light. Anthocyanins and their derivatives are among the most important pigment families in black grapes. The anthocyanin molecule contains a flavylium nucleus, possessing positively charged

oxygen. Due to the existence of conjugated double bonds, the charge is de facto delocalized over the entire cycle, which is stabilized by resonance [18]. On the one hand, Anthocyanins are differentiated by their degree of hydroxylation and methylation, and on the other hand, by the nature of the oses bound to the molecule. Anthocyanidin is the chromophore group of the pigment. In heterosidic form (anthocyanins), these molecules are much more stable than in their aglycon form (anthocyanidins).

Five anthocyanidins are distinguished in grapes and wine by substituents at the R1 and R2 positions (Table 1). Several derivatives are possible depending on the nature of the glucose in position 3: glucose, acetylated glucose, p-coumaroyl glucose, caffeoyl glucose. New anthocyanins acylated with unusual organic acids, such as lactic acid and ferulic acid, have also been identified in trace amounts in some red wines [19]. Within the grape berry, anthocyanins are co-localized with tannins in the thick-walled hypodermic cells of the skin [20,21]. In some so-called "dyer" grape varieties, they are also present in the pulp. They are extracted during alcoholic fermentation and pre- and post-fermentation macerations. Malvidin-3-O glucoside is the major anthocyanin in grapes (70-90%).

Table 1. The chemical structures of anthocyanins.

Anthocyanin	R1	R2
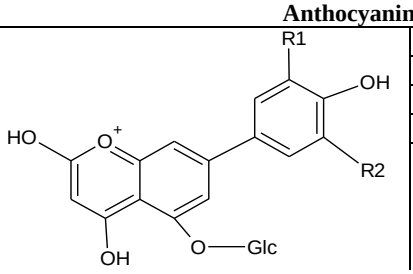 Malvidin-3-O-glucoside	OCH_3	OCH_3
Peonidin-3-O-glucoside	OCH_3	H
Delphinidin-3-O-glucoside	OH	OH
Petunidine-3-O-glucoside	OCH_3	OH
Cyanidin-3-O-glucoside	OH	H

1.1. The balance of anthocyanins as a function of Ph.

The color of an anthocyanin solution is pH-dependent. The flavylium form, which is red, although possessing an electronic deficit, is stable in an acidic environment and changes, when the pH increases, either into a carbinol base (colorless), chalcone (yellow), or quinone base (blue), purple or red pigments located in the skin of the grapes and which are found in the musts. Anthocyanins constitute an important family of organic molecules present, particularly in the berry of red grapes. The main property of anthocyanins is their coloring power. The anthocyanins produced by grapes are distinguished by the surprising simplicity of their structure. We can cite, in particular, the pinot noir, which produces the simplest anthocyanins in all the vegetable kingdom. These pigments belong to the group of chlorophylls and anthocyanins (mainly for black grapes). Among the flavonoids, anthocyanins and flavonols are particularly important in enology since they constitute the grape's red pigments and tannins. Anthocyanins appear during veraison and increase throughout ripening. They reach a maximum around maturity. The concentration of anthocyanins varies considerably depending on the grape variety. The anthocyanins are extracted at the start of fermentation in the aqueous phase. Anthocyanins and grape tannins are very reactive molecules that, as soon as they are extracted from the grape berries in the liquid medium. Free anthocyanins are not very stable. Their content drops noticeably during the first months of aging until disappearing within a few years, although the wine remains red. First of all, this decrease is due to combination reactions with various compounds, in particular tannins. It is then the consequence of degradation reactions due to heat and violent oxidation. Only the anthocyanins combined with the tannins will ensure the stability of the color [22-27]. Anthocyanins are characterized by their

antioxidant properties, which are beneficial to health and, in particular, against cellular aging by improving the elasticity and density of the skin. Recent medical studies also highlight the positive properties of these polyphenolic pigments in preventing cardiovascular accidents and Alzheimer's disease [28-31].

1.2. Flash relaxation to increase the pigment content.

In the grape berry, most of the agents responsible for the color (pigments) and flavor are found in the skin cells of the grain. They are mainly polyphenolic compounds, aroma precursors, tannins, and anthocyanin pigments.

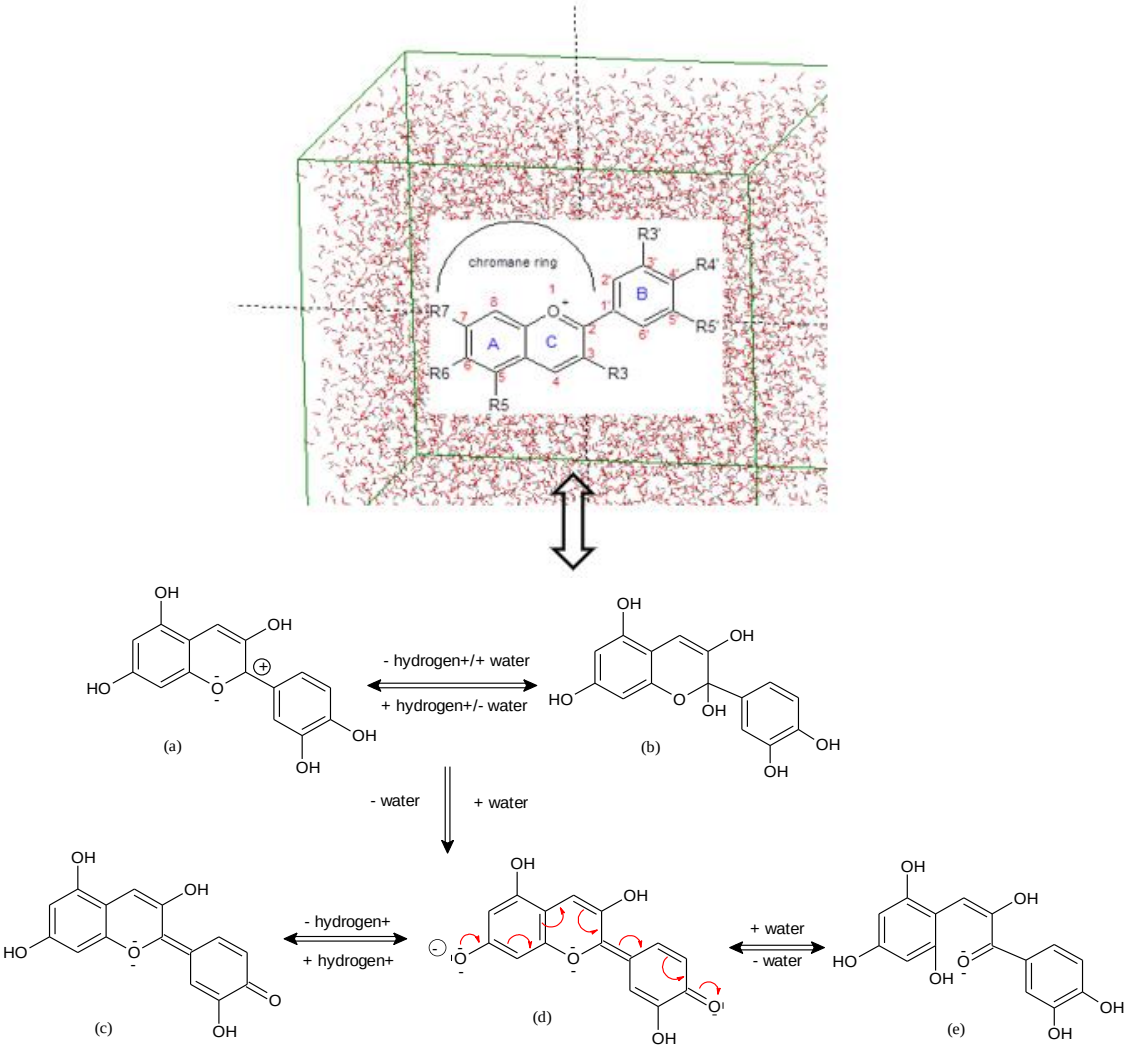

Scheme 1. Mal, Peo, Del, Pet, and Cya in the water toward the appearance of pigments reveal a variety of molecular transformations with the pH changes and generating different colors; (**a)** (Flavylium cation) pH>3 red; (**b)** Carbonyl pseudo base (pH=4-5 colorless); (**c)** anhydrobase (pH= 6-7 violet); (**d)** anhydrobase anion (pH=7-8 blue), (**e)** chalcone (pH>8 yellow)

However, conventional winemaking methods only allow 30 to 50% of this potential to be extracted, the rest being lost in the marc at pressing. A new technique, flash relaxation, increases the polyphenol content by more than 50%. It involves heating the fruit quickly and instantly placing it under a vacuum, promoting the freedom of catching compounds in the cell parts. Trapped inside the cells. So, scientists have shown that the color of anthocyanins in nature differs from H^+ cations, consisting of a weakly acidic medium. At pH of 3, changing the

color makes the complex of colorful anthocyanin cation that changes into colorless or near-colorless samples (Scheme 1).

In fact, these structures are precious edible compounds for health as they are against the known free radicals for what is named "oxidative stress". These are produced naturally by our body and are, to some extent, necessary because they are involved, for example, in the defense against pathogenic viruses and bacteria. However, certain factors such as overexposure to the sun, alcohol, tobacco, stress, and an unbalanced diet can contribute to excessive production of these radicals, causing cell damage and contributing to premature aging of tissues and the development of cardiovascular disease or degenerative diseases such as cancer. To counteract the negative effects of our lifestyle, it is therefore important to adopt a diet rich in antioxidant nutrients such as vitamins A, C, and E, trace elements (copper, selenium, zinc), carotenoids (beta carotene and lycopene), and polyphenols [32-38]. The berries of red fruits are real health allies. They have extraordinary antioxidant power thanks to their polyphenol and vitamin C content, have recognized anti-inflammatory properties, and are a food highly appreciated by our beneficial intestinal bacteria. Among the red fruits with the most powerful antioxidant powers, we find blueberries, mulberries, raspberries, and strawberries.

The exact physiological and physicochemical mechanism of astringency is not yet fully understood, but psychophysical evidence supports that astringency is not a taste. First, the relationship between the intensity of perception and the concentration of monomeric and polymeric tannins is linear over a wide range of concentrations, which is not the case for all the other tastes studied. Second, unlike tastes, the perception of which decreases following repeated ingestions, the sensation of astringency is accentuated under the same conditions. Third, mutual suppression is a fundamental property between all tastes that astringency does not have. Additionally, astringency can be felt on surfaces lacking taste receptors, such as the surface below the lips inside the mouth [39-43].

The origin of the color of the red flavylium A^+ form and the blue AO form of anthocyanins can be found in their structures. Energy with the correct wavelength/frequency can promote an electron from a full orbital to an empty orbital, resulting in a UV-visible spectrum. If the wavelength of the absorbed light falls within the visible region, this compound is colored. Generally, the more a compound is conjugated, the tighter the amount of energy required for the transition and, therefore, the greater the wavelength of light it can absorb. UV-visible spectroscopy can tell us about the conjugations present in a molecule. With fewer than eight conjugated double bonds, the compound only absorbs UV. With more than eight conjugated double bonds, absorption slides into the visible [44].

In the presence of sulfur dioxide (SO_2), solutions of free anthocyanins are strongly disycolourable. In aqueous media, SO_2 combines with water to produce sulfurous acid, which equilibrates according to the following equation [45]:

$$H_2O + SO_2 \overset{pK_{a1}}{\longleftrightarrow} HSO_3^- + H^+ \overset{pK_{a2}}{\longleftrightarrow} SO_3^{2-} + 2H^+$$

The balance of the solution depends mainly on the pH of the medium but also the temperature and the ethanol content. At pH 3.5, 96.3% of the sulfurous acid ($SO_2 + H_2O$) occurs as the hydrogen sulfite anion (HSO_3^-) [46]. The HSO_3^- ion can react with the flavylium cation of the anthocyanin, mainly on the C4 carbon, although theoretically, this is also on the C_2 carbon, leading to the formation of colorless ASO_3H-type compounds [47] (Scheme 2). This substitution would also prevent the condensation of anthocyanins with other molecules. The bleaching effect of SO_2 on combined and polymerized anthocyanins is less or nonexistent [48].

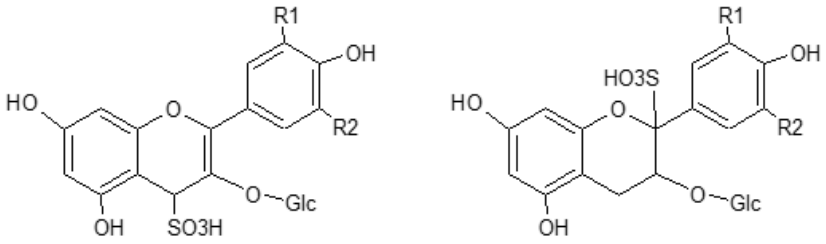

Scheme 2. Structures of colorless ASO_3H form resulting from the reaction between anthocyanins and HSO_3^- ion.

Glińska and his coworkers have illustrated the decrease of potential toxic effects of ACNs through separating M^{n+} chelation of these compounds [49,50].

In these structures, the color expression of the "Del" began red, becoming violet, and then blue as pH and ACN concentrations were maintained, but the Al^{3+} content increased. Chelation of Al^{3+} with Cya has been identified to develop in aqueous samples, pH 2-5, which indicate violet colorations [51].

Buchweitz and his coworkers compared the stability of Al^{3+} chelates of Del-3-rutinoside in American eggplant to that of acylated Cya glycosides, red cabbage, as literature is limited about the stability of acylated ACN metal chelates. They explained that ACN metal complexes are stronger to heat treatment rather than light exposure. Degradation of Del-Al chelates seems jointed to concentration with the rate decreasing over time, in agreement with recent research [52].

In recent research, it has been approved that Al^{3+} in metalloanthocyanins can induce blue color development with Del, having a pyrogallol moiety on the B ring. Still, it is not enough to lead to blue colors with Cya derivatives [53]. Therefore, a theoretical study of the linkage between the electronic and chemical structure of $Mg^{2+}/Al^{3+}/Ga^{3+}/ Sn^{2+}/Cr^{3+}/Fe^{3+}$ by Mal, Peo, Del, Pet, and Cya and their stability has been followed using theoretical and computational methods in water at 300 K.

2. Theory of chelation

The chelation of anthocyanins of Mal, Peo, Del, Pet, and Cya with $Mg^{2+}/Al^{3+}/Ga^{3+}/ Sn^{2+}/Cr^{3+}/Fe^{3+}$ has been studied in this investigation by forming relatively stable complexes in the weak acidified medium with a different pH range. Thus, a series of quantum-theoretical approaches has been done for finding the optimized coordination of [ACN- $Mg^{2+}/Al^{3+}/Ga^{3+}/ Sn^{2+}/Cr^{3+}/Fe^{3+}$] chelation with IR computations and following the Beer-Lambert rule using Gaussian09 program package [54]. It has been indicated that polarization functions into the principal basis set in the calculation show us a significant result in the simulation and modeling approaches. So, IR consequences are the outlook of frequency potential by an analytic methodology that keeps the movement of all atoms at the same time in a vibrant time scale toward a real discussion of molecular vibrant [55-60].

First, optimized geometry coordination of [Cya- $Mg^{2+}/Al^{3+}/Ga^{3+}/ Sn^{2+}/Cr^{3+}/Fe^{3+}$] chelation complexes through their B ring in water at 300K evaluated. Besides, charge electron transfer and thermodynamic properties of [ACN- $Mg^{2+}/Al^{3+}/Ga^{3+}/ Sn^{2+}/Cr^{3+}/Fe^{3+}$] chelation through their B ring in water at 300K have been estimated and compared to each other by different concentrations of H^+ in a simulated solvent model (Figure 1).

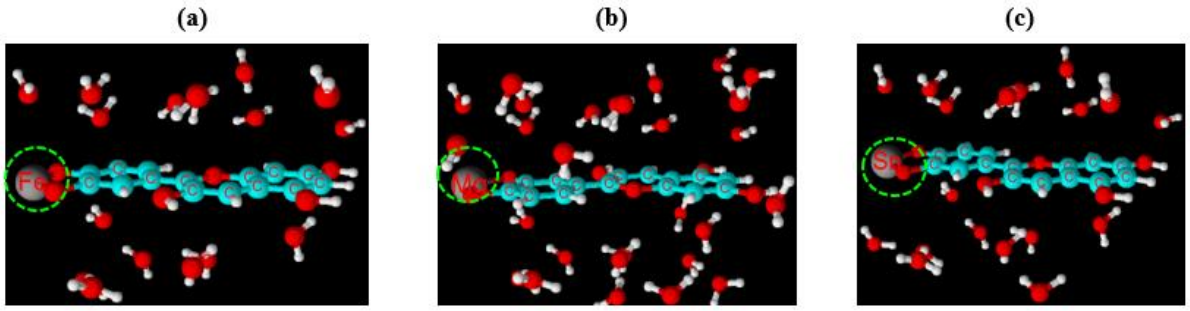

Figure 1. The schematics of (**a**) ACN- Fe^{3+}; (**b**) ACN- Mg^{2+}; (**c**) ACN- Sn^{2+} due to the bond length of O ⋯ Mn+ and bond angle of O ⋯ Mn+⋯ O in the molecular structure.

In this work, the data has been achieved from thermodynamic parameters of ΔG, ΔH, and ΔS for the solute-solvent model of [ACN- Mg^{2+}/Al^{3+}/Ga^{3+}/ Sn^{2+}/Cr^{3+}/Fe^{3+}] chelation in water at 300K. Therefore, for accomplishing a stable structure of [ACN- Mg^{2+}/Al^{3+}/Ga^{3+}/ Sn^{2+}/Cr^{3+}/Fe^{3+}] chelation of Mal, Peo, Del, Pet, and Cya pigments, geometry coordination with IR computations have been run; the intensity and frequency of the IR modes were evaluated with the QM approach, and the basic infrared vibrant were measured by their changes of minimized energy in H_2O. So, thermodynamical analysis pursues infrared information data. So, computed data was run at different basis sets to achieve correct equilibrium coordinated results and frequency data for each of the certain structures. It is assumed that another polarization and diffuse levels in the basis set used in the calculation direct us to the special development of the consequences of the theory. The simulation indicates the approaches that produce a common model template at a special temperature by computing all physicochemical properties among the partition function [56].

3. Results and Discussion

The use of data from back grape sequencing of three anthocyanin pigments of Mal, Peo, Del, Pet, and Cya have been calculated using theoretical methods to evaluate order to identify molecular actors involved in the transport of anthocyanins in metal chelation with cations of Mg^{2+}/Al^{3+}/Ga^{3+}/ Sn^{2+}/Cr^{3+}/Fe^{3+} in different pH and evaluated using Gaussian09 in a water medium (Figure 2). In this project, three anthocyanin pigments of Mal, Peo, Del, Pet, and Cya have been estimated using theoretical methods to measure the effect of metal chelation of different plants, including factorial excess of Mg^{2+}/Al^{3+}/Ga^{3+}/ Sn^{2+}/Cr^{3+}/Fe^{3+} in different pH and evaluated by IR spectroscopy using Gaussian09 in water media at 300K. The thermodynamical characterizations gibs free energy, enthalpy entropy, ΔG, ΔH, ΔS, Electronic Energy, Core-Core Interaction, IR properties frequency spectrums, anthocyanin amount, and pH conduct us towards final color and stability (Table 2 and Figure 2) [54].

Table 2. Thermochemical factors of Cya, Del, Mal, Pel, Peo, pet in water at 300K.

Pigment	ΔG	ΔH	ΔS ×10^{-2}	$E_{electronic}$	$E_{core-core}$	lnK ×10^{-5}
Cya	-2.85×10^5	-1.54×10^3	9.44	-2.80×10^6	2.51×10^6	2.85
Del	-2.92×10^5	-1.57×10^3	9.69	-2.89×10^6	2.60×10^6	4.90
Mal	-2.11×10^5	-9.07×10^2	7.00	-1.86×10^6	1.65×10^6	3.54
Pel	-2.45×10^5	-1.26×10^3	8.14	-2.25×10^6	2.01×10^6	1.37
Peo	-2.72×10^5	-1.42×10^3	9.03	-2.61×10^6	2.33×10^6	4.56
Pet	-2.80×10^5	-1.47×10^3	9.28	-2.75×10^6	2.47×10^6	4.69

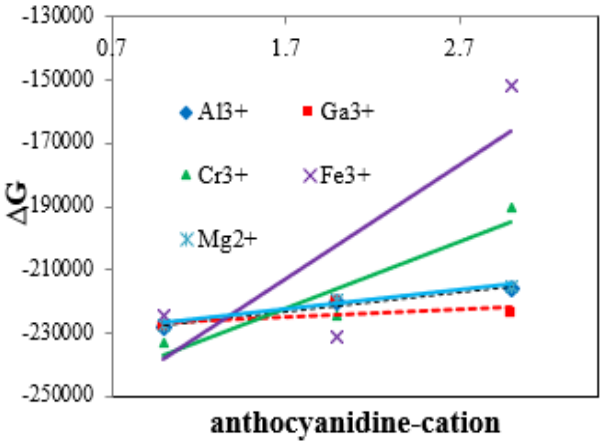

Figure 2. Flactuation of Gibbs free energy (Δ*G*, kcal/mol) of [anthocyanin- $Mg^{2+}/Al^{3+}/Ga^{3+}/ Sn^{2+}/Cr^{3+}/Fe^{3+}$] chelation in water at 330K.

Six anthocyanin pigments of cyanidin (Cya), delphinidin (Del), malvidin (Mal), pelargonidin (Pel), peonidin (Peo), and petunidin (Pet) have been evaluated using theoretical methods to evaluate the dielectric solvent effect on the stability of these anthocyanins water at 300 K. As it has been shown, a vibrational calculation with its eigenvector for finding thermodynamic parameters and physical properties of anthocyanins including ΔG,ΔH, ΔS lnK, Core-Core Interaction, and Electronic Energy has been calculated by Gaussian09 in water at 300K (Table 2 and Figure 2) [60].

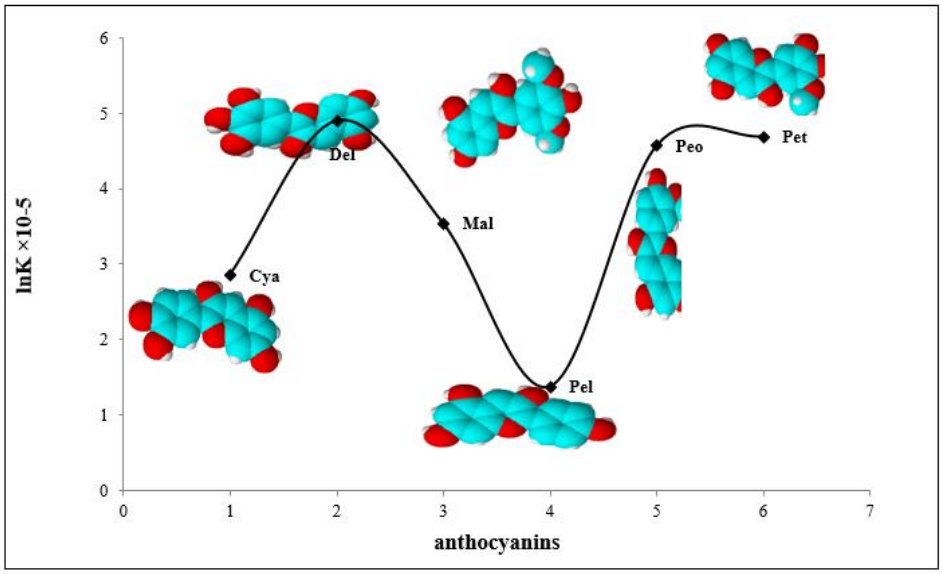

Figure 3. The calculated equilibrium constant (K) of anthocyanin pigments of Cya, Del, Mal, Pel, Peo, Pet in water at 300K.

The difference between these subclasses is revealed in double bonds and carbonyl groups in the C ring in water media that approves the stability and color of anthocyanins pigments in a weak acidic condition (Figure 3).

The absorbance (A) of six anthocyanins pigments of Cya, Del, Mal, Pel, Peo, Pet in a water medium has been measured in Table 3 based on the beer-lambert rule; the absorbance is directly proportional to the concentration (c/ $molL^{-1}$) of the solution for the compounds through Beer-Lambert equations of $A = \log_{10} (I_o/I)$ and $A = \varepsilon lc$.

Table 3. Calculated absorbance (A), Frequency, and Dipole moment of anthocyanin-metal chelation of Cya, Del, and Pet in various pH.

pH	A	Frequency	Dipole	A	Frequency	Dipole	A	Frequency	Dipole	A	Frequency	Dipole	A	Frequency	Dipole
Cya	**Mg^{2+}**			**Ga^{3+}**			**Cr^{3+}**			**Fe^{3+}**			**Al^{3+}**		
1.17	0.10	3922.70	3.05	0.25	3924.86	18.65	0.22	3926.30	9.94	0.13	3924.71	0.25	0.25	3924.86	18.65
1.30	1.20	3927.39	3.24	1.32	3925.22	16.74	0.96	3931.09	8.39	1.06	3926.28	1.32	1.32	3925.22	16.74
1.40	1.21	3927.39	1.53	0.64	3926.23	16.35	0.65	3926.20	10.31	0.95	3926.28	0.64	0.64	3926.23	16.35
1.48	1.89	4014.50	5.27	1.87	4008.35	13.82	0.68	3926.21	8.59	1.19	3928.35	1.87	1.87	4008.35	13.82
1.54	1.89	4012.12	3.91	1.85	4007.68	6.69	1.90	4009.28	9.59	1.90	4012.01	1.85	1.85	4007.68	6.69
pH Del	**Mg^{2+}**			**Ga^{3+}**			**Cr^{3+}**			**Fe^{3+}**			**Al^{3+}**		
1.17	0.70	3926.53	6.71	0.42	3925.41	18.78	0.89	3933.41	9.04	0.89	3767.49	7.90	3.59	3925.80	1617.19
1.30	1.20	3929.42	3.67	1.25	3927.6	14.94	0.89	3933.41	9.04	3.93	3945.54	1907.47	1.07	3929.67	1745.15
1.40	2.81	5816.27	22.60	1.24	3927.92	12.99	1.07	3935.24	6.40	0.89	3928.67	6.87	1.12	3929.62	16.10
1.48	1.24	3930.14	4.91	3.75	4040.77	2293.99	1.92	4017.84	7.38	1.92	4018.25	5.54	1.86	4015.05	17.01
1.54	1.92	4018.29	3.75	1.90	4014.13	13.14	1.84	4015.40	9.03	1.95	4016.15	6.38	1.80	4012.90	16.86
pH Pet	**Mg^{2+}**			**Ga^{3+}**			**Cr^{3+}**			**Fe^{3+}**			**Al^{3+}**		
1.2	0.39	3925.49	8.2	0.61	3926.05	17.77	1.47	3767.37	26.67	0.39	3925.49	8.2	1.22	3764.23	22.84
1.30	3.59	3925.48	7.89	0.57	3925.90	16.37	0.27	3926.38	9.77	3.59	3925.48	7.89	3.59	3930.10	1.22
1.40	0.97	3938.03	6.59	1.04	3936.28	15.78	1.02	3944.92	9.34	0.97	3938.03	6.59	8.50	7744.65	1935.27
1.48	0.96	3941.18	5.34	1.07	3935.38	2473.38	0.86	3940.57	6.89	0.96	3941.18	5.34	1.06	3953.97	16.27
1.54	1.00	3940.83	6.52	1.89	4013.77	12.82	0.92	3943.45	6.21	1.00	3940.83	6.52	1.96	4013.69	15.92

The difference in ΔH_R among [ACN- $Mg^{2+}/Al^{3+}/Ga^{3+}/ Sn^{2+}/Cr^{3+}/Fe^{3+}$] chelation complexes (Figure 4) has been explored through double bonds and carbonyl groups by the B ring chelated of Cya, Del, and Pet anthocyanins in water that illustrates the stability and color of [ACN- $Mg^{2+}/Al^{3+}/Ga^{3+}/ Sn^{2+}/Cr^{3+}/Fe^{3+}$] chelation of Cya, Del, and Pet pigments in a weakly acidic solution. The highest chelate stability with different ACNs indicates that ACN-metal chelation can produce a varied range of colors under acidic pH with efficiency for food consumption. The results of ΔH_R for the formation of [Cya, Del, Pet- $Mg^{2+}/Al^{3+}/Ga^{3+}/ Sn^{2+}/Cr^{3+}/Fe^{3+}$] chelation complexes have been extracted in Figure 4 and data from Table 2.

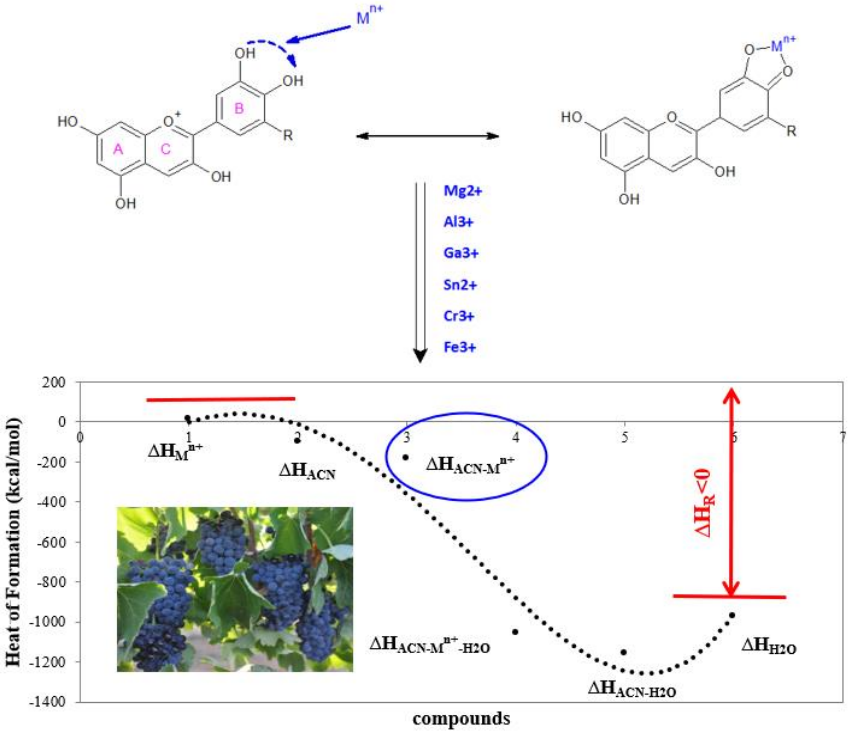

Figure 4. Changes of enthalpy of reaction (ΔH_R) for formation of [ACN- $Mg^{2+}/Al^{3+}/Ga^{3+}/ Sn^{2+}/Cr^{3+}/Fe^{3+}$ - chelation] complexes in water medium.

In the present project, the Beer-Lambert rule has been applied for minimized structures of [Cya, Del, Pet- $Mg^{2+}/Al^{3+}/Ga^{3+}/ Sn^{2+}/Cr^{3+}/Fe^{3+}$] attached to explain the linkage of identified molecules for indicating the stability and a limitation of color through their electronic compounds in H_2O media with different concentrations of H^+ (Table 3). The absorbance (A) of the anthocyanins- $Al^{3+}/Ga^{3+}/Cr^{3+}/Fe^{3+}$ /Mg^{2+} ion chelation of Cya, Del, and Pet pigments in H_2O molecules has been modeled, which relates to concentration (c/ mol/L) of H^+. The data has been introduced based on $A = \log_{10} (I_o/I) = \varepsilon lc$ (Table3 and Figure 5a, b). A big increase in absorbance might be considered to transform the colorless states of anthocyanin to those that absorb and reflect visible light and the M^{n+} induced attached to ACN compounds (Figure 5a, b).

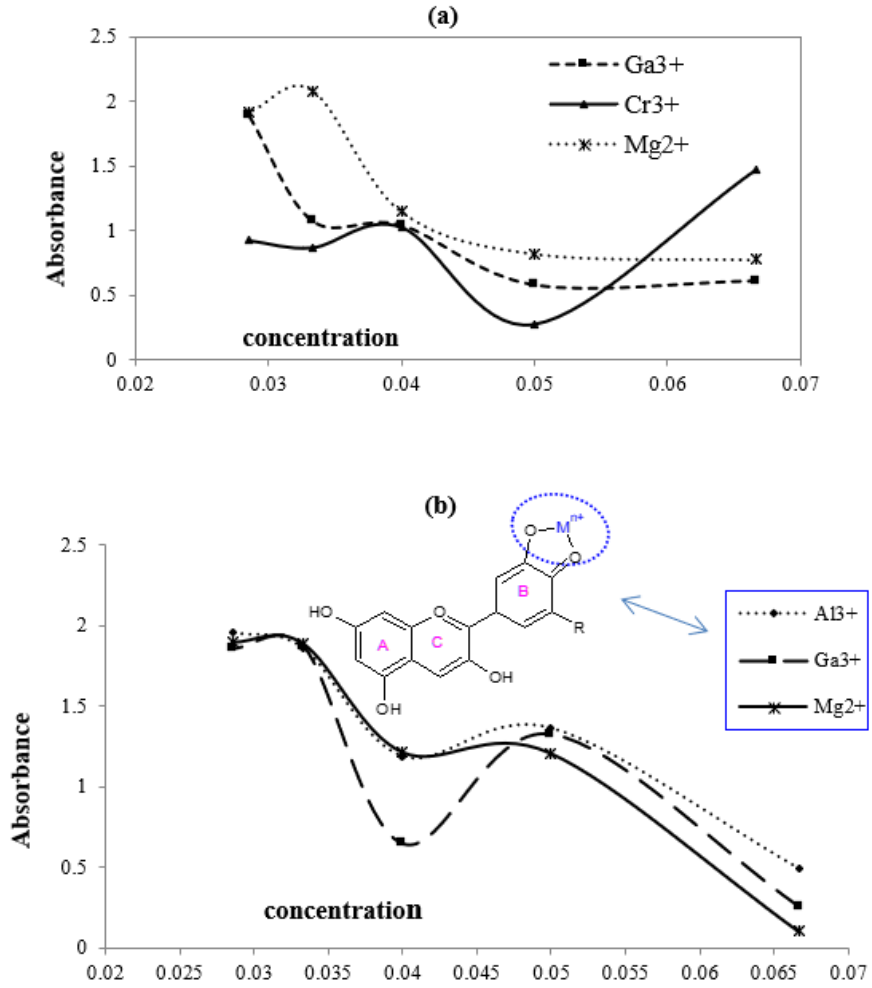

Figure5. Changes of absorbance (A) versus concentration (c) through beer-lambert law for; (**a)** [Pet- $Al^{3+}/Ga^{3+}/ Mg^{2+}$]chelation and (**b)** [Cya- $Al^{3+}/Ga^{3+}/ Mg^{2+}$] chelation in the weak acidic media by different concentrations of H^+ at 300K.

It has been seen the absorbance of Cya, Del, and Pet with Mg^{2+} cation. Still, the shiftings were of the magnitude by a function in establishing anthocyanin ACN into macromolecules like the function of Mg^{2+} cation in metalloanthocyanins foundation [53]. So, Mg^{2+} cation is the divalent metal cation applied in this research which is an essential M^{n+} to life status and usually attached to anthocyanin in plants without any electrons in d orbitals. It can produce some metalloanthocyanins with the empty orbitals of d or f [62]. Mg^{2+} was explored to function in the stereochemical configurations of Cya, Del, and Pet anthocyanins. To discover the impacts of Al3+ salt on food origin, ACN was measured to understand the blue color development of metallo-ACN better. In calculations, Al^{3+} was identified to displace Mg^{2+} in ACN- Mg^{2+}

complexes, Cya based, and produces more stable complexes [63]. This M^{n+} has also even been estimated as a key to evaluating Cya, Del, and Pet in ACN extracts from edible sources. Similar to Mg^{2+}, Al^{3+} also lacks electrons in *d* orbitals but is trivalent when ionized. In all pH, the frequency, intensity, absorbance, and thermodynamics properties of ACN-chelation were found to be significantly different with each metal treatment (Al^{3+}/Ga^{3+}/Mg^{2+}). It has been seen that by increasing the pH, the frequency of [Cya-Al^{3+}/Ga^{3+}/Mg^{2+}] chelation increases between pH ≈1.1-1.5. The maximum frequency of Al^{3+} treated acylated Cya was greater, indicating the development of bluer colors, especially in higher pH with effects on their visible light absorbance (Figure 6).

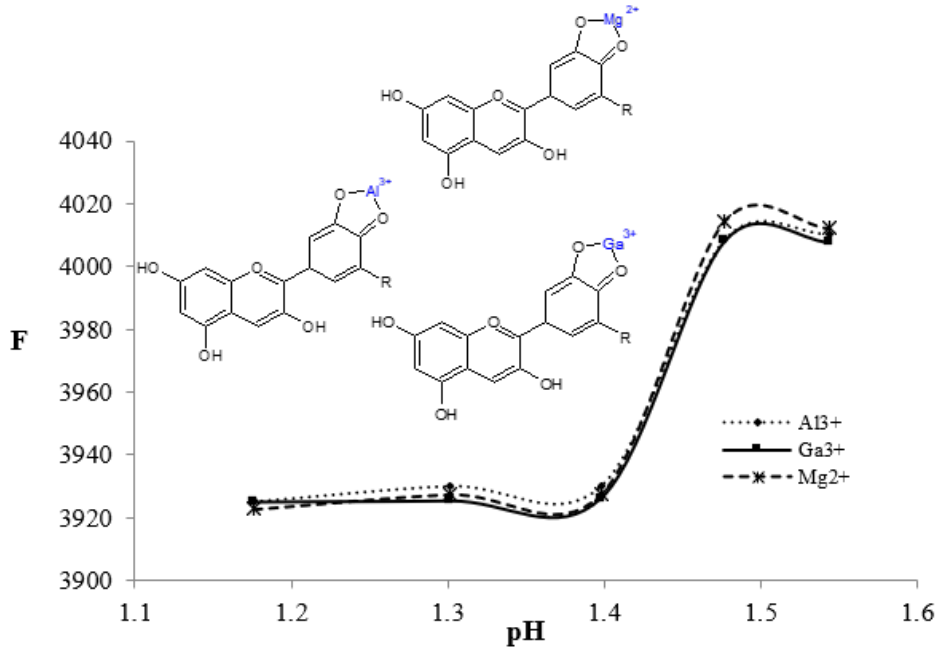

Figure 6. Changes of frequency (F) versus pH for [Cya-Al^{3+}/Ga^{3+}/Mg^{2+}] chelation in the weak acidic media by different concentrations of H^+ at 300K.

Although we have little information about the interaction of ACN with Cr^{3+}, it is trivalent M^{n+} having electrons in d orbitals, whereby adding the Cr^{3+} to the ACN of this research was also explored to approve the spectra of absorbance. The mean frequency of the ACN of both sources in all pH was accomplished to be different metal cation compounds. Similar trends occurred with Cr^{3+}, where the F_{max} of chelated Cya and Del were greater while it has been shown the larger Fmax of the ACN with Cr^{3+} compared to Al^{3+}in chelation by Cya and Pet. Like Al^{3+}, the impacts of iron chelated to ACN were investigated to be better characterized to generate some ACN based blue colorations. Fe^{3+} is an important role in many of the known pigment macromolecules [53]. Those metalloanthocyanins with Cya chromophores need Fe^{3+} to generate blue hues, but those based on Del chromophores can precede blue colors. So, it has been seen ACN formed bonds with Fe^{3+} producing the highest shift of frequency and absorbance compared to other metalloanthocyanins (Figure 6). As has been seen in Table 3, the physical properties of high frequency and dipole moment for ACN-metal cation chelated, including Cya-Al^{3+}, Del-Al^{3+}, and Pet-Al^{3+} have been calculated in weakly acidic media extracted from the infrared computational method, which shows a high deviation of absorbance for [Al^{3+}- chelation] of Del pigment.

The frequency achieved by IR vibrational spectra has shown that the normal mode of the active sites is due to anthocyanin-metal cation chelation of Cya-Al^{3+}, Del-Al^{3+}, and Pet-

Al^{3+} in minimized weak acidic media, indicating the resistance and color of these compounds. The principal frequency vibrational modes have been illustrated based on the stability and color of various anthocyanin-metal cation chelation (Table 3). In the next step, the atomic charge of indicated atoms in [ACN- Mg^{2+}/Al^{3+}/Ga^{3+}/ Sn^{2+}/Cr^{3+}/Fe^{3+}] chelation has been evaluated as the active parts of the molecules which play an important role in the electron charge transfer toward producing a range of various colors in water (Table 4).

Table 4. Atomic charge for Oxygen atoms in molecules of [ACN-Mg^{2+}/Al^{3+}/Ga^{3+}/ Sn^{2+}/Cr^{3+}/Fe^{3+}-chelation] in water medium.

Cyanidin					
atom	**Mg^{2+}**	**Ga^{3+}**	**Cr^{3+}**	**Fe^{3+}**	**Al^{3+}**
O10	-0.42	-0.37	-0.02	-0.16	-0.36
O^{+}17	-0.13	-0.16	-0.13	-0.14	-0.13
O24	-0.20	-0.23	-0.21	-0.21	-0.18
O25	-0.22	-0.22	-0.21	-0.22	-0.21
O26	-0.21	-0.21	-0.21	-0.21	-0.21
O27	-0.39	-0.34	0.07	-0.13	-0.33
M^{n+}31	0.76	0.76	-0.45	0.07	-0.02
Delphinidin					
atom	**Mg^{2+}**	**Ga^{3+}**	**Cr^{3+}**	**Fe^{3+}**	**Al^{3+}**
O9	-0.39	-0.56	0.00	-0.14	-0.32
O^{+}16	-0.13	-0.13	-0.13	-0.13	-0.13
O23	-0.20	-0.18	-0.21	-0.20	-0.18
O24	-0.21	-0.20	-0.20	-0.21	-0.20
O25	-0.21	-0.21	-0.21	-0.21	-0.21
O26	-0.40	-0.63	0.06	-0.12	-0.33
O30	-0.21	-0.18	-0.21	-0.21	-0.19
M^{n+}32	0.76	0.64	-0.42	0.04	0.04
Petunidin					
atom	**Mg^{2+}**	**Ga^{3+}**	**Cr^{3+}**	**Fe^{3+}**	**Al^{3+}**
O^{+}7	-0.13	-0.13	-0.13	-0.13	-0.13
O17	-0.40	-0.57	0.03	-0.13	-0.33
O18	-0.39	-0.63	0.04	-0.17	-0.33
O19	-0.20	-0.19	-0.21	-0.21	-0.19
O20	-0.21	-0.19	-0.21	-0.20	-0.21
O21	-0.22	-0.21	-0.22	-0.22	-0.21
O30	-0.15	-0.12	-0.15	-0.15	-0.13
M^{n+}35	0.76	0.65	-0.42	0.0	0.03

In Figure 7 it has been plotted the changes in atomic charge of labeled oxygen atoms and metal cations through optimized [ACN- Mg^{2+}/Al^{3+}/Ga^{3+}/ Sn^{2+}/Cr^{3+}/Fe^{3+}] chelation.

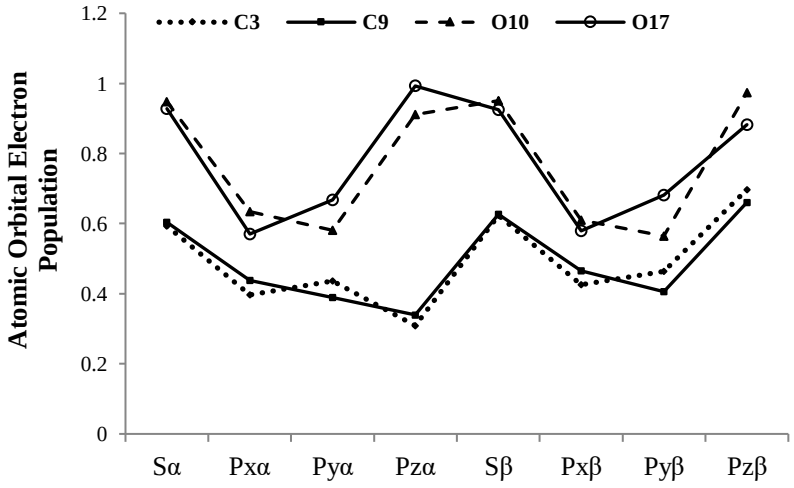

Figure 7. Comparison of atomic charge versus labeled oxygen atoms and metal cations through optimized [ACN- Mg2+/Al3+/Ga3+/ Sn2+/Cr3+/Fe3+] chelation in water.

The outlook of Figure 7 recommends the reason for existing observed various results of [ACN- Mg^{2+}/Al^{3+}/Ga^{3+}/ Sn^{2+}/Cr^{3+}/Fe^{3+}] chelation which are attached to the status of active cites of precise oxygens and metal cations in these compounds, which pass the charge of electrons in the aromatic cyclic chain. Therefore, the partial charges and spin density have been gained by matching the electrostatic potential to a fixed charge of O^{+}_{17}, O^{+}_{16}, and O^{+}_{7} cations for Cya-M^{n+} (31), Del-M^{n+} (32), and Pet-M^{n+}(35), respectively (Table 4 & Figure 7); therefore, the electrophilic groups of Cya, Del anthocyanin pigments conduct us to find the reason for the stability and the activity of these compounds in the natural products.

4. Conclusions

In this paper, the anthocyanins of cyanidin (Cya), delphinidin (Del), and petunidin (Pet) with a big linkage in the active part of these complexes by metal cations of (Mg^{2+}/Al^{3+}/Ga^{3+}/ Sn^{2+}/Cr^{3+}/Fe^{3+}) produce a different range of colors under acidic pH; as divalent Mg^{2+} cation has introduced diverse physicochemical parameters concerning its minimized coordination as oxygen - Mg^{2+} ≈ (1.9Å) and oxygen - Mg^{2+} - oxygen ≈ (112º) while it has been pointed out oxygen - M^{3+} ≈ (1.8Å) and oxygen - M^{3+} - oxygen ≈ (120º) for trivalent metal cations of (Mg^{2+}, Al^{3+}, Ga^{3+}, Sn^{2+}, Cr^{3+}, and Fe^{3+}) metal cations with more metal ions produced big shifts in the color, stability, and foundation.

Besides, we have discovered that [anthocyanin- metal cations of (Mg^{2+}, Al^{3+}, Ga^{3+}, Sn^{2+}, Cr^{3+}, and Fe^{3+})] chelated is founded on the axes of active parts of identified oxygens and metal cations in these molecules. At the same time, the electronic charges differ in aromatic cyclic chains in the presence of a high dielectric constant of water compared to gas. The partial charges and spin density have been estimated by installing the electrostatic potential to pierce the charge of O^{+}_{17}, O^{+}_{16}, and O^{+}_{7} cations for cyanidin-M^{n+}(31), delphinidin-M^{n+} (32), and petunidin-M^{n+}(35), respectively related to the electrophilic properties of cyanidin, delphinidin, and petunidin which explain the stability and the activity of these molecules in the natural structures. Basically, anthocyanins can be attached to the M^{n+} while denotes the shift in their spectra of absorbance and frequency, which are influenced by several parameters such as the anthocyanin crystal and pH, which is the medium parameter in the identified color of the solutions, and also the atomic configuration of the metal cations.

So, the divalent Mg^{2+} cation was indicated to influence ACN approximately by enhancing electron density in diverse pH; Sn^{2+} ≈ Fe^{3+}≈ Ga^{3+}> Al^{3+}> Cr^{3+}>> Mg^{2+}.

Using Beer-Lambert law on anthocyanin- metal cations of (Mg^{2+}, Al^{3+}, Ga^{3+}, Sn^{2+}, Cr^{3+}, and Fe^{3+})] chelated of cyanidin, delphinidin, and petunidin pigments in Iranian black grape applying theoretical approaches discusses the absorbance parameter in two diverse conditions of water and gas and then shows the minimized stabilization energy and the stable coordination which have been influenced by infrared theoretical simulation toward the thermodynamical characterization and the electronic structure of optimized [anthocyanin- metal cations of (Mg^{2+}, Al^{3+}, Ga^{3+}, Sn^{2+}, Cr^{3+}, and Fe^{3+})] cluster chelation in Iranian black grape resulting of metal chelation.

The data have indicated such foundations of [anthocyanin-metal cations of (Mg^{2+}, Al^{3+}, Ga^{3+}, Sn^{2+}, Cr^{3+}, and Fe^{3+})] chelated in Iranian black grape by sharp parts of electrophilic molecules in weakly acidic media with different concentrations of H^{+} which are the most active particles at the applied compounds in this project.

Funding

This research received no external funding.

Acknowledgments

In successfully completing this paper and its research, the authors are grateful to Kastamonu University for their support through the library, the laboratory, and scientific websites.

Conflicts of Interest

The authors declare no conflict of interest.

References

1. Cháirez-Ramírez, M.H.; de la Cruz-López, K.G.; García-Carrancá, A. Polyphenols as Antitumor Agents Targeting Key Players in Cancer-Driving Signaling Pathways. *Front. Pharmacol*. **2021**, *12*, 710304, https://doi.org/10.3389/fphar.2021.710304.
2. Morata, A.; Escott, C.; Loira, I.; López, C.; Palomero, F.; González, C. Emerging Non-Thermal Technologies for the Extraction of Grape Anthocyanins. *Antioxidants* **2021**, *10*, 1863, https://doi.org/10.3390/antiox10121863.
3. Kumara, K.; Srivastava, S.; Sharanagatb, V.S. Ultrasound assisted extraction (UAE) of bioactive compounds from fruit and vegetable processing by-products: A review. Ultrason. *Sonochemistry* **2021**, *70*, 105325, https://doi.org/10.1016/j.ultsonch.2020.105325.
4. Gao, Y.; Ji, Y.; Wang, F.; Li, W.; Zhang, X.; Niu, Z.; Wang, Z. Optimization the extraction of anthocyanins from blueberry residue by dual-aqueous phase method and cell damage protection study. *Food Sci. Biotechnol.* **2021**, *30*, 1709-1719, https://doi.org/10.1007/s10068-021-00994-w.
5. Moirangthem, K.; Ramakrishna, P.; Amer, M.H.; Tucker, G.A. Bioactivity and anthocyanin content of microwave-assisted subcritical water extracts of Manipur black rice (Chakhao) bran and straw. *Future Foods* **2021**, *3*, 100030, https://doi.org/10.1016/j.fufo.2021.100030.
6. Carrera, C.; Aliaño-González, M.J.; Valaityte, M.; Ferreiro-González, M.; Barbero, G.F.; Palma, M. A Novel Ultrasound-Assisted Extraction Method for the Analysis of Anthocyanins in Potatoes (Solanum tuberosum L.). *Antioxidants* **2021**, *10*, 1375, https://doi.org/10.3390/antiox10091375.
7. Bagade, S.B.; Patil, M. Recent Advances in Microwave Assisted Extraction of Bioactive Compounds from Complex Herbal Samples: A Review. *Crit. Rev. Anal. Chem.* **2021**, *51*, 138-149, https://doi.org/10.1080/10408347.2019.1686966.
8. Korpacheva, S.; Serasutdinova, K.; Lomovsky, I.; Chugunova, O. Technological Aspects of Obtaining Melanin and Powder from Buckwheat Hull and Their Use in Food Technology. *E3S Web Conf.* **2021**, *296*, 07007, https://doi.org/10.1051/e3sconf/202129607007.
9. Yi ˘git, Ü.; Yolaçaner, E.T.; Hamzalıo ˘glu, A.; Gökmen, V. Optimization of microwave-assisted extraction of anthocyanins in red cabbage by response surface methodology. *J. Food Process. Preserv*. **2021**, *46*, e16120, https://doi.org/10.1111/jfpp.16120.
10. Odabas, H.I.; Koca, I. Simultaneous separation and preliminary purification of anthocyanins from Rosa pimpinellifolia L. fruits by microwave assisted aqueous two-phase extraction. *Food Bioprod. Process*. **2021**, *125*, 170-180, https://doi.org/10.1016/j.fbp.2020.11.007.
11. Pazir, F.; Kocak, E.; Turan, F.; Ova, G. Extraction of anthocyanins from grape pomace by using supercritical carbon dioxide. *J. Food Process. Preserv.* **2021**, *45*, e14950, https://doi.org/10.1111/jfpp.14950.
12. Wang, Y.; Ye, Y.; Wang, L.; Yin, W.; Liang, J. Antioxidant activity and subcritical water extraction of anthocyanin from raspberry process optimization by response surface methodology. *Food Biosci*. **2021**, *44*, 101394, https://doi.org/10.1016/j.fbio.2021.101394.
13. Teixeira, R.F.; Benvenutti, L.; Burin, V.M.; Gomes, T.M.; Ferreira, S.R.S.; Ferreira-Zielinski, A.A. An eco-friendly pressure liquid extraction method to recover anthocyanins from broken black bean hulls. *Innov. Food Sci. Emerg. Technol.* **2021**, *67*, 102587, https://doi.org/10.1016/j.ifset.2020.102587.

14. Andrade, T.A.; Hamerski, F.; Fetzer, D.E.L.; Roda-Serrat, M.C.; Corazza, M.L.; Norddahl, B.; Errico, M. Ultrasound-assisted pressurized liquid extraction of anthocyanins from Aronia melanocarpa pomace. *Sep. Purif. Technol.* **2021**, *276*, 119290, https://doi.org/10.1016/j.seppur.2021.119290.
15. Serea, D.; Râpeanu, G.; Constantin, O.E.; Bahrim, G.E.; Stănciuc, N.; Croitoru, C. Ultrasound and enzymatic assisted extractions of bioactive compounds found in red grape skins băbească neagră (vitis vinifera) variety. *Ann. Univ. Dunarea Jos Galati Fascicle VI Food Technol.* **2021**, *45*, 9-25, https://doi.org/10.35219/foodtechnology.2021.1.01.
16. Monajjemi, M.; Farahani, N.; Mollaamin, F. Thermodynamic study of solvent effects on nanostructures: phosphatidylserine and phosphatidylinositol membranes. *Phys Chem Liquids* **2012**, *50*, 161-172, https://doi.org/10.1080/00319104.2010.527842.
17. Bakhshi, K.; Mollaamin, F.; Monajjemi, M. Exchange and Correlation Effect of Hydrogen Chemisorption on Nano V(100) Surface: A DFT Study by Generalized Gradient Approximation (GGA). *Journal of Computational and Theoretical Nanoscience* **2011**, *8*, 763-768, https://doi.org/10.1166/jctn.2011.1750.
18. Lee, V.S.; Nimmanpipug, P.; Mollaamin, F.; Kungwan, N.; Thanasanvorakun, S.; Monajjemi, M. Investigation of single wall carbon nanotubes electrical properties and normal mode analysis: Dielectric effects. *Russian Journal of Physical Chemistry A* **2009**, *83*, 2288-2296, https://doi.org/10.1134/S0036024409130184.
19. Faisal Manzoor, M.; Ahmed, Z.; Ahmad, N.; Karrar, E.; Rehman, A.; Aadil, R.M.; Al-Farga, A.; Waheed Iqbal, M.; Rahaman, A.; Zeng, X.A. Probing the combined impact of pulsed electric field and ultra-sonication on the quality of spinach juice. *J. Food Process. Preserv.* **2021**, *45*, e15475, https://doi.org/10.1111/jfpp.15475.
20. Yildiz, S.; Pokhrel, P.R.; Unluturk, S.; Barbosa-Cánovas, G.V. Changes in Quality Characteristics of Strawberry Juice After Equivalent High Pressure, Ultrasound, and Pulsed Electric Fields Processes. *Food Eng. Rev.* **2021**, *13*, 601-612, https://doi.org/10.1007/s12393-020-09250-z.
21. Hamadou, M.H.; Kerkatou, M.; Zucal, C.; Bisio, A.; Provenzani, A.; Inga, A.; Menad, A.; Benayache, S.; Benayache, F.; Ameddah, S. Limonium duriusculum (de Girard) kuntze exhibits anti-inflammatory effect via NF-κB pathway modulation. *Braz. Arch. Biol. Techn.* **2021**, *64*, e21200179, https://doi.org/10.1590/1678-4324-2021200179.
22. Zhang, W.; Shen, Y.; Li, Z.; Xie, X.; Gong, E.S.; Tian, J.; Si, X.; Wang, Y.; Gao, N.; Shu, C.; Meng, X.; Li, B.; Liu, R.H. Effects of high hydrostatic pressure and thermal processing on anthocyanin content, polyphenol oxidase and β-glucosidase activities, color, and antioxidant activities of blueberry (Vaccinium Spp.) puree. *Food Chem.* **2021**, *342*, 128564, https://doi.org/10.1016/j.foodchem.2020.128564.
23. Monajjemi, M.; Afsharnezhad, S.; Jaafari, M.R.; Mirdamadi, S.; Mollaamin, F.; Monajemi, H. Investigation of energy and NMR isotropic shift on the internal rotation Barrier of Θ4 dihedral angle of the DLPC: A GIAO study. *Chemistry* **2008**, *17*, 1.
24. Ghalandari, B.; Monajjemi, M.; Mollaamin, F. Theoretical Investigation of Carbon Nanotube Binding to DNA in View of Drug Delivery. *J. Comput. Theor. Nanosci.* **2011**, *8*, 1212-1219, https://doi.org/10.1166/jctn.2011.1801.
25. Monajjemi, M.; Baie, M.T.; Mollaamin, F. Interaction between threonine and cadmium cation in $[Cd(Thr)_n]^{2+}$ (n = 1–3) complexes: density functional calculations. *Russian Chemical Bulletin* **2010**, *59*, 886-889, https://doi.org/10.1007/s11172-010-0181-5.
26. Xue, H.; Tan, J.; Li, Q.; Tang, J.; Cai, X. Ultrasound-Assisted Enzymatic Extraction of Anthocyanins from Raspberry Wine Residues: Process Optimization, Isolation, Purification, and Bioactivity Determination. *Food Anal. Methods* **2021**, *14*, 1369–1386, https://doi.org/10.1007/s12161-021-01976-8.
27. Li, X.; Zhu, F.; Zeng, Z. Effects of different extraction methods on antioxidant properties of blueberry anthocyanins. *Open Chem.* **2021**, *19*, 138-148, https://doi.org/10.1515/chem-2020-0052.
28. Gonçalves, A.C.; Nunes, A.R.; Falcão, A.; Alves, G.; Silva, L.R. Dietary effects of anthocyanins in human health: A comprehensive review. *Pharmaceuticals* **2021**, *14*, 690, https://doi.org/10.3390/ph14070690.
29. Monajjemi,M.; Khaleghian, M.; Tadayonpour, N.; Mollaamin, F. The effect of different solvents and temperatures on stability of single-walled carbon nanotube: a QM/MD study. *Int. J. Nanosci.* **2010**, *9*, 517, https://doi.org/10.1142/S0219581X10007071.
30. Ge, X.; Jing, L.; Zhao, K.; Su, C.; Zhang, B.; Zhang, Q.; Han, L.; Yu, X.; Li, W. The Phenolic Compounds Profile, Quantitative Analysis and Antioxidant Activity of Four Naked Barley Grains with Different Color. *Food Chem.* **2021**, *335*, 127655, https://doi.org/10.1016/j.foodchem.2020.127655.

31. Ni, Y.; Chen, H.; Liu, D.; Zeng, L.; Chen, P.; Liu, C. Discovery of genes involved in anthocyanin biosynthesis from the rind and pith of three sugarcane varieties using integrated metabolic profiling and RNA-seq analysis. *BMC Plant Biol*. **2021**, *21*, 1-15, https://doi.org/10.1186/s12870-021-02986-8.
32. Vukoja, J.; Buljeta, I.; Pichler, A.; Šimunovi'c, J.; Kopjar, M. Formulation and Stability of Cellulose-Based Delivery Systems of Raspberry Phenolics. *Processes* **2021**, *9*, 90, https://doi.org/10.3390/pr9010090.
33. Dhua, S.; Kumar, K.; Kumar, Y.; Singh, L.; Sharanagat, V.S. Composition, Characteristics and Health Promising Prospects of Black Wheat: A Review. *Trends Food Sci Technol* **2021**, *112*, 780-794, https://doi.org/10.1016/j.tifs.2021.04.037.
34. Zhang, Y.; Yin, L.; Huang, L.; Tekliye, M.; Xia, X.; Li, J.; Dong, M. Composition, Antioxidant Activity, and Neuroprotective Effects of Anthocyanin-Rich Extract from Purple Highland Barley Bran and Its Promotion on Autophagy. *Food Chem.* **2021**, *339*, 127849, https://doi.org/10.1016/j.foodchem.2020.127849.
35. Campos, M.G.; Frigerio, C.; Bobi¸s, O.; Urcan, A.C.; Gomes, N.G.M. Infrared Irradiation Drying Impact on Bee Pollen: Case Study on the Phenolic Composition of Eucalyptus globulus Labill and Salix atrocinerea Brot. Pollens. *Processes* **2021**, *9*, 890, https://doi.org/10.3390/pr9050890.
36. de Souza Guedes, L.; Martinez, R.M.; Bou-Chacra, N.A.; Velasco, M.V.R.; Rosado, C.; Baby, A.R. An Overview on Topical Administration of Carotenoids and Coenzyme Q10 Loaded in Lipid Nanoparticles. *Antioxidants* **2021**, *10*, 1034, https://doi.org/10.3390/antiox10071034.
37. Trapani, A.; Guerra, L.; Corbo, F.; Castellani, S.; Sanna, E.; Capobianco, L.; Monteduro, A.G.; Manno, D.E.; Mandracchia, D.; Di Gioia, S.; Conese, M. Cyto/Biocompatibility of Dopamine Combined with the Antioxidant Grape Seed-Derived Polyphenol Compounds in Solid Lipid Nanoparticles. *Molecules* **2021**, *26*, 916, https://doi.org/10.3390/molecules26040916.
38. Qin, J.; Zhao, C.; Wang, S.; Gao, N.; Wang, X.; Na, X.; Wang, X.; Bi, Y. PIF4-PAP1 interaction affects MYB-bHLH-WD40 complex formation and anthocyanin accumulation in Arabidopsis. *J. Plant Physiol.* **2021**, *268*, 153558, https://doi.org/10.1016/j.jplph.2021.153558.
39. Mackon, E.; Jeazet Dongho Epse Mackon, G.C.; Ma, Y.; Haneef Kashif, M.; Ali, N.; Usman, B.; Liu, P. Recent insights into anthocyanin pigmentation, synthesis, trafficking, and regulatory mechanisms in rice (Oryza sativa L.) Caryopsis. *Biomolecules* **2021**, *11*, 394, https://doi.org/10.3390/biom11030394.
40. Koo, Y.; Poethig, R.S. Expression pattern analysis of three R2R3-MYB transcription factors for the production of anthocyanin in different vegetative stages of Arabidopsis leaves. *Appl. Biol. Chem*. **2021**, *64*, 5, https://doi.org/10.1186/s13765-020-00584-0.
41. Jiu, S.; Guan, L.; Leng, X.; Zhang, K.; Haider, M.S.; Yu, X.; Zhu, X.; Zheng, T.; Ge, M.; Wang, C. The role of VvMYBA2r and VvMYBA2w alleles of the MYBA2 locus in the regulation of anthocyanin biosynthesis for molecular breeding of grape (Vitis spp.) skin coloration. *Plant Biotechnol. J.* **2021**, *19*, 1216-1239, https://doi.org/10.1111/pbi.13543.
42. Khaleghian, M.; Zahmatkesh, M.; Mollaamin, F.; Monajjemi, M. Investigation of Solvent Effects on Armchair Single-Walled Carbon Nanotubes: A QM/MD Study. *Fuller. Nanotub. Carbon Nanostructures* **2011**, *19*, 251-261, https://doi.org/10.1080/15363831003721757.
43. Mackon, E.; Jeazet Dongho Epse Mackon, G.C.; Ma, Y.; Haneef Kashif, M.; Ali, N.; Usman, B.; Liu, P. Recent insights into anthocyanin pigmentation, synthesis, trafficking, and regulatory mechanisms in rice (Oryza sativa L.) Caryopsis. *Biomolecules* **2021**, *11*, 394, https://doi.org/10.3390/biom11030394.
44. Monajjemi, M.; Mahdavian, L.; Mollaamin, F.; Khaleghian, M. Interaction of Na, Mg, Al, Si with carbon nanotube (CNT): NMR and IR study. *Russ. J. Inorg. Chem.* **2009**, *54*, 1465-1473, https://doi.org/10.1134/S0036023609090216.
45. Monajjemi, M.; Noei, M.; Mollaamin, F. Design of fMet-tRNA and calculation of its bonding properties by quantum mechanics. *Nucleosides, Nucleotides and Nucleic Acids* **2010**, *29*, 9, https://doi.org/10.1080/15257771003781642.
46. Rao, M.J.; Ahmed, U.; Ahmed, M.H.; Duan, M.; Wang, J.; Wang, Y.; Wang, L. Comparison and quantification of metabolites and their antioxidant activities in young and mature leaves of sugarcane. *ACS Food Sci. Technol.* **2021**, *1*, 362-373, https://doi.org/10.1021/acsfoodscitech.0c00133.
47. Mura, P.; Maestrelli, F.; D'Ambrosio, M.; Luceri, C.; Cirri, M. Evaluation and Comparison of Solid Lipid Nanoparticles (SLNs) and Nanostructured Lipid Carriers (NLCs) as Vectors to Develop Hydrochlorothiazide Effective and Safe Pediatric Oral Liquid Formulations. *Pharmaceutics* **2021**, *13*, 437, https://doi.org/10.3390/pharmaceutics13040437.

48. Qin, L.; Sun, L.; Wei, L.; Yuan, J.; Kong, F.; Zhang, Y.; Miao, X.; Xia, G.; Liu, S. Maize SRO1e represses anthocyanin synthesis through regulating the MBW complex in response to abiotic stress. *Plant J.* **2021**, *105*, 1010-1025, https://doi.org/10.1111/tpj.15083.
49. Luo, D.; Xiong, C.; Lin, A.; Zhang, C.; Sun, W.; Zhang, J.; Yang, C.; Lu, Y.; Li, H.; Ye, Z. SlBBX20 interacts with the COP9 signalosome subunit SlCSN5-2 to regulate anthocyanin biosynthesis by activating SlDFR expression in tomato. *Hortic. Res.* **2021**, *8*, 1-12, https://doi.org/10.1038/s41438-021-00595-y.
50. Li, Q.; Kou, M.; Li, C.; Zhang, Y.-G. Comparative transcriptome analysis reveals candidate genes involved in anthocyanin biosynthesis in sweetpotato (Ipomoea batatas L.). *Plant Physiol. Biochem.* **2021**, *158*, 508-517, https://doi.org/10.1016/j.plaphy.2020.11.035.
51. Tahan, A.; Mollaamin, F.; Monajjemi, M. Thermochemistry and NBO analysis of peptide bond: Investigation of basis sets and binding energy. *Russian Journal of Physical Chemistry A* **2009**, *83*, 587-597, https://doi.org/10.1134/S003602440904013X.
52. Rao, M.J.; Zuo, H.; Xu, Q. Genomic insights into citrus domestication and its important agronomic traits. *Plant Commun.* **2021**, *2*, 100138, https://doi.org/10.1016/j.xplc.2020.100138.
53. Przybylska-Balcerek, A.; Szablewski, T.; Szwajkowska-Michałek, L.; Swierk, D.; Cegielska-Radziejewska, R.; Krejpcio, Z.; Suchowilska, E.; Tomczyk, Ł.; Stuper-Szablewska, K. Sambucus Nigra Extracts-Natural Antioxidants and Antimicrobial Compounds. *Molecules* **2021**, *26*, 2910, https://doi.org/10.3390/molecules26102910.
54. Yue, X.; Zhao, Y.; Ma, X.; Jiao, X.; Fang, Y.; Zhang, Z.; Ju, Y. Effects of leaf removal on the accumulation of anthocyanins and the expression of anthocyanin biosynthetic genes in Cabernet Sauvignon (Vitis vinifera L.) grapes. *J. Sci. Food Agric.* **2021**, *101*, 3214-3224, https://doi.org/10.1002/jsfa.10951.
55. Naing, A.H.; Kim, C.K. Abiotic stress-induced anthocyanins in plants: Their role in tolerance to abiotic stresses. *Physiol. Plant.* **2021**, *172*, 1711-1723, https://doi.org/10.1111/ppl.13373.
56. Frisch, M.J.; Trucks, G.W.; Schlegel, H.B.; Scuseria, G.E.; Robb, M.A.; Cheeseman, J.R.; Scalmani, G.; et al. Gaussian, Inc., Wallingford CT. **2009**.
57. Mollaamin, F.; Monajjemi, M. Harmonic Linear Combination and Normal Mode Analysis of Semiconductor Nanotubes Vibrations. *J. Comput. Theor. Nanosci.* **2015**, *12*, 1030-1039, https://doi.org/10.1166/jctn.2015.3846.
58. Monajjemi, M.; Mollaamin, F.; Gholami, M.R.; Yoosbashizadeh, H.; Sadrnezhad, S.K.; Passdar, H. Quantum Chemical Parameters of Some Organic Corrosion Inhibitors, Pyridine, 2-Picoline 4-Picoline and 2, 4-Lutidine, Adsorption at Aluminum Surface in Hydrocholoric and Nitric Acids and Comparison Between Two Acidic Media. *Main Group Met. Chem.* **2003**, *26*, 349-362, https://doi.org/10.1515/MGMC.2003.26.6.349.
59. Zadeh, MAA.; Lari, H.; Kharghanian, L.; Balali, E.; Khadivi, R.; Yahyaei, H.; Mollaamin, F.; Monajjemi, M. Density Functional Theory Study and Anti-Cancer Properties of Shyshaq Plant: In View Point of Nano Biotechnology. *J. Comput. Theor. Nanosci.* **2015**, *12*, 4358-4367, https://doi.org/10.1166/jctn.2015.4366.
60. Mollaamin, F.; Ilkhani, A.; Sakhaei, N.; Bonsakhteh, B.; Faridchehr, A.; Tohidi, S.; Monajjemi, M. Thermodynamic and Solvent Effect on Dynamic Structures of Nano Bilayer-Cell Membrane: Hydrogen Bonding Study. *J. Comput. Theor. Nanosci.* **2015**, *12*, 3148-3154, https://doi.org/10.1166/jctn.2015.4046.
61. Mollaamin, F.; Monajjemi, M.; Salemi, S.; Baei, M.T. A Dielectric Effect on Normal Mode Analysis and Symmetry of BNNT Nanotube. *Fuller. Nanotub. Carbon Nanostructures* **2011**, *19*, 182-196, https://doi.org/10.1080/15363831003782932.
62. Sarasia, E.M.; Afsharnezhad, S.; Honarparvar, B.; Mollaamin, F.; Monajjemi, M. Theoretical study of solvent effect on NMR shielding tensors of luciferin derivatives. *Phys Chem Liquids* **2011**, *49*, 561-571, https://doi.org/10.1080/00319101003698992.
63. Ye, G.; Zheng, Z.; Zhou, Y.; Pu, X.; Su, W.; Guo, H.; Wang, J. The MYB transcription factor LrAN2, from Lycium ruthenicum, led to enhanced accumulation of anthocyanins and modified profile of the total glycoalkaloids in potato. *Plant Cell Tissue Organ Cult.* **2021**, *147*, 519-528, https://doi.org/10.1007/s11240-021-02144-w.
64. Chen, T.; Li, B.; Shu, C.; Tian, J.; Zhang, Y.; Gao, N.; Cheng, Z.; Xie, X.; Wang, J. Combined effect of thermosonication and high hydrostatic pressure on bioactive compounds, microbial load, and enzyme activities of blueberry juice. *Food Sci. Technol. Int.* **2021**, *25*, 33765872, https://doi.org/10.1177/10820132211004316.
65. Rezende, Y.R.R.S.; Nogueira, J.P.; Silva, T.O.M.; Barros, R.G.C.; de Oliveira, C.S.; Cunha, G.C.; Gualberto, N.C.; Rajan, M.; Narain, N. Enzymatic and ultrasonic-assisted pretreatment in the extraction of bioactive

compounds from Monguba (Pachira aquatic Aubl) leaf, bark and seed. *Food Res. Int.* **2021**, *140*, 109869, https://doi.org/10.1016/j.foodres.2020.109869.